The Astrophysical Journal, 595:94–108, 2003 September 20

LOW-REDSHIFT DAMPED Lyα GALAXIES TOWARD THE QUASARS B2 0827+243, PKS 0952+179, PKS 1127−145, AND PKS 1629+120[1]

Sandhya M. Rao, Daniel B. Nestor, and David A. Turnshek
Department of Physics and Astronomy, University of Pittsburgh, Pittsburgh, PA 15260; rao@everest.phyast.pitt.edu

Wendy M. Lane
US Naval Research Laboratory, 4555 Overlook Avenue SW, Code 7600A, Washington, DC 20375

Eric M. Monier
Department of Astronomy, Ohio State University, Columbus, OH 43210

and

Jacqueline Bergeron
Institut d'Astrophysique de Paris, 98bis Boulevard Arago, F 75014, Paris, France
Received 2002 November 14; accepted 2003 June 4

ABSTRACT

We present optical and near-infrared ground-based imaging results on four low-redshift damped Lyα (DLA) galaxies. The corresponding DLA systems were discovered in our *Hubble Space Telescope* spectroscopic surveys for DLA lines in known strong Mg II absorption-line systems toward the quasars B2 0827+243 ($z_{\rm DLA} = 0.525$), PKS 0952+179 ($z_{\rm DLA} = 0.239$), PKS 1127−145 ($z_{\rm DLA} = 0.313$), and PKS 1629+120 ($z_{\rm DLA} = 0.532$). Two of the four DLA galaxies have confirmed slit redshifts, one has a photometric redshift consistent with the absorption-line redshift, and the fourth identification is based on the galaxy's proximity to the quasar sight line. The DLA galaxies span a mixture of morphological types from patchy, irregular, and low surface brightness to spiral galaxies. The luminosities range from $0.02L_K^*$ to $1.2L_K^*$. We also discovered several extremely red objects (EROs) in two of these fields and discuss the possibility that they are associated with the DLA galaxies. These observations add to the small but growing list of DLA galaxies at low redshift. At the present time, 14 DLA galaxies in the redshift range $0.05 \lesssim z \lesssim 1$ have been studied. The distributions of DLA galaxy properties for these 14 cases are discussed, and some important trends emerge. Low-luminosity dwarf galaxies with small impact parameters dominate this small sample. Also, four of the five highest column density systems, which dominate in the determination of the cosmological neutral gas mass density, arise in low surface brightness dwarf galaxies. Zwaan et al. have shown that only 15% of the neutral gas at the present epoch is contained in low surface brightness galaxies. Thus, if the low-redshift DLA galaxy trends hold up with larger samples, it would indicate that a different population of objects is responsible for the bulk of the neutral hydrogen gas in the universe at $z \approx 0.5$.

Subject headings: quasars: absorption lines — quasars: individual (B2 0827+243, PKS 0952+179, PKS 1127−145, PKS 1629+120)

1. INTRODUCTION

Surveys for damped Lyα (DLA) absorption lines in the spectra of quasi-stellar objects (QSOs), or quasars, have been used to study the distribution of neutral hydrogen in the universe (see, e.g., Wolfe et al. 1986; Lanzetta et al. 1991; Rao & Turnshek 2000, hereafter RT2000). These studies indicate that the DLA systems, historically defined to have $N_{\rm H\,I} \geq 2 \times 10^{20}$ atoms cm^{-2}, trace the bulk of the neutral gas mass in the universe up to at least redshift $z \approx 3.5$. At $z > 3.5$, inclusion of lower $N_{\rm H\,I}$ systems in the sub-DLA regime may be necessary to encompass the bulk of the H I mass (Péroux et al. 2001). In either case, study of the DLA systems reveals the H I gas production and consumption history over a large fraction of the age of the universe. Thus, DLA galaxies, which are identified by virtue of their H I gas cross sections, are the only population of cosmological objects that simultaneously reveal information relevant to both star formation and H I gas production and consumption, making them crucial for understanding the evolutionary history of neutral gas. Galaxies selected in optical/IR surveys are generally only used to track the star formation history of the universe (see, e.g., Madau, Pozzetti, & Dickinson 1998). How these two distinctly selected populations (i.e., H I cross section–selected vs. optical/IR–selected) are related is as yet unclear.

Ground-based imaging of high-redshift DLA galaxies has had limited success, either because the quasar point-spread function (PSF) prevents the detection of objects very close to the quasar sight line, or because the DLA galaxy is simply too faint, or both. In addition, the faintness of any candidates close to the quasar sight line makes it difficult to obtain confirming redshifts. Imaging of high-redshift DLA galaxies with the *Hubble Space Telescope* (*HST*) has been more successful at identifying faint candidates close to the

[1] Based on observations obtained with the 3.5 m WIYN Telescope on Kitt Peak, operated for the NSF by the Association of Universities for Research in Astronomy (AURA), Inc. (WIYN is a joint facility of University of Wisconsin, Indiana University, Yale University, and NOAO), the Infrared Telescope Facility, which is operated by the University of Hawaii under a cooperative agreement with the National Aeronautics and Space Administration, the Hiltner 2.4 m Telescope on Kitt Peak, operated by MDM Observatory (this is a joint facility of University of Michigan, Dartmouth College, Ohio State University, and Columbia University), and the 3.6 m European Southern Observatory New Technology Telescope on La Silla, Chile.

Report Documentation Page

Form Approved
OMB No. 0704-0188

1. REPORT DATE	2. REPORT TYPE	3. DATES COVERED
SEP 2003		**00-00-2003 to 00-00-2003**

4. TITLE AND SUBTITLE	5a. CONTRACT NUMBER
Low-Redshift Damped Lycx Galaxies Toward the Quasars B2 0827+243, PKS 0952+179, PKS 1127-145, and PKS 1629+120	5b. GRANT NUMBER
	5c. PROGRAM ELEMENT NUMBER
6. AUTHOR(S)	5d. PROJECT NUMBER
	5e. TASK NUMBER
	5f. WORK UNIT NUMBER
7. PERFORMING ORGANIZATION NAME(S) AND ADDRESS(ES) **Naval Research Laboratory,Code 7213,4555 Overlook Avenue, SW,Washington,DC,20375**	8. PERFORMING ORGANIZATION REPORT NUMBER
9. SPONSORING/MONITORING AGENCY NAME(S) AND ADDRESS(ES)	10. SPONSOR/MONITOR'S ACRONYM(S)
	11. SPONSOR/MONITOR'S REPORT NUMBER(S)

12. DISTRIBUTION/AVAILABILITY STATEMENT
Approved for public release; distribution unlimited

13. SUPPLEMENTARY NOTES

14. ABSTRACT

15. SUBJECT TERMS

16. SECURITY CLASSIFICATION OF:			17. LIMITATION OF ABSTRACT	18. NUMBER OF PAGES	19a. NAME OF RESPONSIBLE PERSON
a. REPORT **unclassified**	b. ABSTRACT **unclassified**	c. THIS PAGE **unclassified**		**15**	

quasar sight lines, but only a few of these have confirmed redshifts. See Warren et al. (2001 and references therein) for details. The main conclusion of these studies has been that most high-redshift DLA galaxies are underluminous in comparison to the Lyman break galaxy population.

Morphologies, colors, and stellar populations of low-redshift DLA galaxies can be more easily studied, but progress has been slow mainly because of their rarity. *HST* observations along many quasar sight lines in traditional spectroscopic survey mode are needed to find a single DLA system at $z < 1.65$ (see, e.g., Jannuzi et al. 1998). However, since it is known from optical studies that all high-redshift DLA systems have accompanying Mg II absorption, we have to a large extent circumvented this problem in our *HST* surveys by targeting quasars known to have Mg II absorption lines in their spectra (Rao, Turnshek, & Briggs 1995; RT2000). We reasoned that if this held at high redshift, it would also be the case at low redshift, since galaxies only increase their metallicities with age. In fact, during the course of this work we uncovered a new empirical criterion for finding DLA systems. Approximately half of the systems with Mg II λ2796 rest equivalent width $W_0^{\lambda 2796} > 0.5$ Å, as well as Fe II $W_0^{\lambda 2600} > 0.5$ Å, have DLA absorption (RT2000), and the number of DLA systems that do not meet this criterion appears to be insignificant. As a result, these targeted surveys have now nearly tripled the number of DLA galaxies known at $z < 1.65$ to $\approx$30, which is in comparison to the $\approx$80 at $z > 1.65$ that have been discovered and confirmed in optical quasar spectra. Of course, once the strong Mg II–Fe II criterion is used to identify low-redshift DLA candidate systems at $z < 1.65$, *HST* UV spectroscopy is still required to obtain a reasonably precise measurement of $N_{\rm HI}$, which is then used to confirm or refute the candidate as lying in the DLA regime.

The few published imaging studies of low-redshift ($z < 1.65$) DLA galaxies have revealed a mix of morphological types. Burbidge et al. (1996) obtained *HST* images along the sight line toward the BL Lac object AO 0235+165, which contains a $z = 0.524$ DLA system selected on the basis of 21 cm absorption; they found a significant number of galaxies near the sight line, including an active galactic nucleus (AGN) that has broad absorption line (BAL) features and a fainter, late-type galaxy. Both of these objects are at the DLA redshift, but the late-type galaxy has a smaller impact parameter. Le Brun et al. (1997) presented *HST* images of six low-redshift DLA galaxies that included spirals, low surface brightness (LSB) galaxies, and compact objects, with luminosities ranging from $0.07L^*$ to $1.4L^*$. Three of these six were selected on the basis of 21 cm absorption. In another case, no evidence for a galaxy at the $z = 0.656$ DLA redshift toward the quasar 3C 336 was found, despite very deep ground-based and *HST* imaging (Steidel et al. 1997; Bouché et al. 2001). Also, previously, we presented results on two DLA galaxies toward the quasar OI 363 at redshifts $z = 0.091$ and 0.221 (Rao & Turnshek 1998; Turnshek et al. 2001). The $z = 0.091$ galaxy is an LSB galaxy with apparent spiral structure nearly centered on the quasar sight line, while the $z = 0.221$ galaxy is an early-type dwarf spiral at an impact parameter of 20 kpc. Here, we present more ground-based imaging results on three low-redshift DLA systems, which we discovered in our *HST* Cycle 6 survey toward the quasars B2 0827+243, PKS 0952+179, and PKS 1127−145, as well as one new DLA system, which we discovered in our *HST* Cycle 9 survey toward the quasar PKS 1629+120. We continue to find that the DLA galaxies are drawn from a mix of morphological types, but, with the increased total sample size, observed trends are becoming more compelling. In the last section of this paper, we summarize results from imaging studies of a cosmological sample ($z > 0.05$) of 14 DLA galaxies with $z \lesssim 1$ known at the time of publication.

The paper is organized as follows. Details of our observations are given in § 2. The identification of the DLA galaxies, their photometric properties, and some details of the fields containing the four new low-redshift DLA galaxies are described in § 3. A discussion and the conclusions are presented in § 4. All distance-related quantities are calculated using a cosmology with $\Omega_M = 1.0$, $\Omega_\Lambda = 0.0$, and $H_0 = 65$ km s^{-1} Mpc^{-1}. When luminosities are expressed in terms of L^*, we assume $M_B^* = -20.9$ (Marinoni et al. 1999), $M_R^* = -21.2$ (Lin et al. 1996), and $M_K^* = -24.5$ (Loveday 2000), where the magnitudes have been converted to our adopted cosmology.

2. OBSERVATIONS

The four quasar fields were observed during the period between 1998 December and 2001 June. Optical images were obtained with the MDM Observatory 2.4 m Hiltner Telescope on Kitt Peak, using the 1024×1024 Templeton CCD (0.″285 pixel^{-1}), and with the 3.5 m WIYN telescope on Kitt Peak. Observations with the WIYN telescope were made in both classical scheduling mode, using the Mini-Mosaic 4096×2048 SITe CCD pair (0.″141 pixel^{-1}), and queue mode, by the WIYN queue observing team using a 1024×1024 Tektronix CCD (0.″195 pixel^{-1}). The near-infrared images were obtained at the 3.0 m NASA IRTF on Mauna Kea, using NSFCAM in combination with a 256×256 InSb detector array (0.″30 pixel^{-1}), and the 3.6 m ESO NTT on La Silla, using SOFI, which uses a 1024×1024 HgCdTe detector array (0.″292 pixel^{-1}). The images were processed using the recommended procedures, and standard-star observations were used to calibrate the photometry. The observations are summarized in Table 1. We note that some of the observations listed in Table 1 were taken under less than ideal conditions, but were still useful for confirmation of some of the derived results. Some of the images were smoothed to enhance LSB features, and these are shown in § 3. The smoothing was performed using a Gaussian with a $\sigma \approx 1$ pixel. On average, this degraded the seeing by 20%. The smoothed images were used to delineate the LSB features and set the aperture for doing the photometry, but photometric measurements were made on the unsmoothed images. Faint features in the smoothed images were deemed real if they were detected in at least two filters at greater than a 2 σ level of significance. Limiting 3 σ surface brightnesses and seeing measurements for the final combined (unsmoothed) images used in the analysis presented here are given in Table 2.

3. DLA GALAXY IDENTIFICATION AND PHOTOMETRY

As detailed below, two of the DLA galaxies have confirmed slit redshifts, one has a photometric redshift consistent with the DLA absorption redshift, and one is

TABLE 1
JOURNAL OF IMAGING OBSERVATIONS

QSO Field	Filter	Telescope	Observation Dates	Exposure Time (minutes)
B2 0827+243.....	*U*	MDM	1999 Nov 13, 14	100
	B	WIYN	1999 Jan 18	54
	R	WIYN	1999 Jan 18	15
	I	MDM	1999 Nov 14	28
	K	IRTF	1999 Apr 27	62
PKS 0952+179.....	*U*	MDM	1999 Feb 17–20	180
	B	MDM	1999 Feb 18, 20	60
	R	MDM	1999 Feb 19, 20	75
	R	WIYN	1999 Mar 20	27
	J	NTT	1999 Jan 2	60
	K_s	NTT	1999 Jan 2	60
	K	IRTF	1998 Dec 12	20
	K	IRTF	2000 Mar 6	63
PKS 1127−145.....	*U*	MDM	1999 Feb 18, 19	120
	B	MDM	1999 Feb 19, 20	60
	R	MDM	1999 Feb 18–20	80
	I	MDM	1999 Nov 13	14
	I	MDM	2001 Feb 26	30
	J	NTT	1999 Jan 2	80
	K	IRTF	1998 Dec 13	60
	K	IRTF	1999 Apr 28	63
PKS 1629+120.....	*U*	WIYN	2001 Jun 25, 27	60
	B	MDM	2000 Sep 29	45
	R	MDM	2000 Sep 29, 30	45
	J	IRTF	2000 Sep 30	50
	K	IRTF	2000 Sep 29	60

identified based on its proximity to the quasar sight line. It should be kept in mind that the degree of confidence for any "identification" of a DLA galaxy is variable, with the confidence being highest when the candidate DLA galaxy has a low impact parameter to the QSO sight line *and* there is a confirming slit spectrum showing that it is at the DLA system redshift. However, even when the confidence is relatively high, it is possible that a fainter galaxy or a galaxy with a smaller impact parameter might be the actual DLA absorber. We proceed with the assumption that a neutral gas cloud (or clouds along the line of sight) associated with the galaxy we identify as the DLA galaxy is the site of the DLA absorption.

When possible, bright stars in the field were used to model the quasar PSF, which was then subtracted before any photometric measurements were made. This was sometimes not possible in the IRTF images, since there were no bright stars in the small field of view (77″) and no PSF star was observed separately.

3.1. *B2 0827+243*

This quasar sight line contains a DLA system at $z = 0.525$, with column density $N_{\rm HI} = (2.0 \pm 0.2) \times 10^{20}$ atoms cm^{-2} (RT2000). Figure 1 shows $\approx 30'' \times 30''$ *B*, *R*, *I*, and *K* images of this field. The quasar PSFs have been subtracted and the residuals masked out. The galaxy 6″ to the east of the sight line, labeled G1, is identified as the DLA galaxy. Steidel et al. (2002) report a spectroscopic redshift of $z = 0.5258$ for G1. They also present an *HST*-WFPC2 F702W image of this field and note the possible presence of a satellite galaxy $\approx 2''$ west-northwest of the center of G1. We a posteriori found a hint of a southwestern extension to G1 in our smoothed *I*-band image (see inset in Fig. 1). Of course, our *I*-band image was obtained in 1.″1 seeing, compared to the $\approx 0.''1$ seeing of the *HST* image. Thus, the satellite noted by Steidel et al. (2002) is unresolved and is not distinct from G1 in our ground-based image. Instead, it is possible that the southwestern extension we detect is an

TABLE 2
3 σ SURFACE BRIGHTNESS LIMITS (μ) AND SEEING MEASUREMENTS (Θ)

	μ (mag arcsec^{-2})						Θ[a] (arcsec)					
FIELD	μ_U	μ_B	μ_R	μ_I	μ_J	μ_K	Θ_U	Θ_B	Θ_R	Θ_I	Θ_J	Θ_K
B2 0827+243.....	24.0	25.1	24.1	22.9	...	19.6	1.3	1.0	0.8	1.1	...	0.7
PKS 0952+179.....	24.2	24.8	24.9	...	22.2	20.8	1.2	1.1	0.7	...	0.7	0.9
PKS 1127−145.....	24.0	25.0	24.5	...	22.8	20.4	0.9	1.2	0.9	...	0.7	0.8
PKS 1629+120.....	23.6	24.6	24.2	...	21.1	20.4	1.3	1.3	1.2	...	1.0	1.0

[a] FWHM.

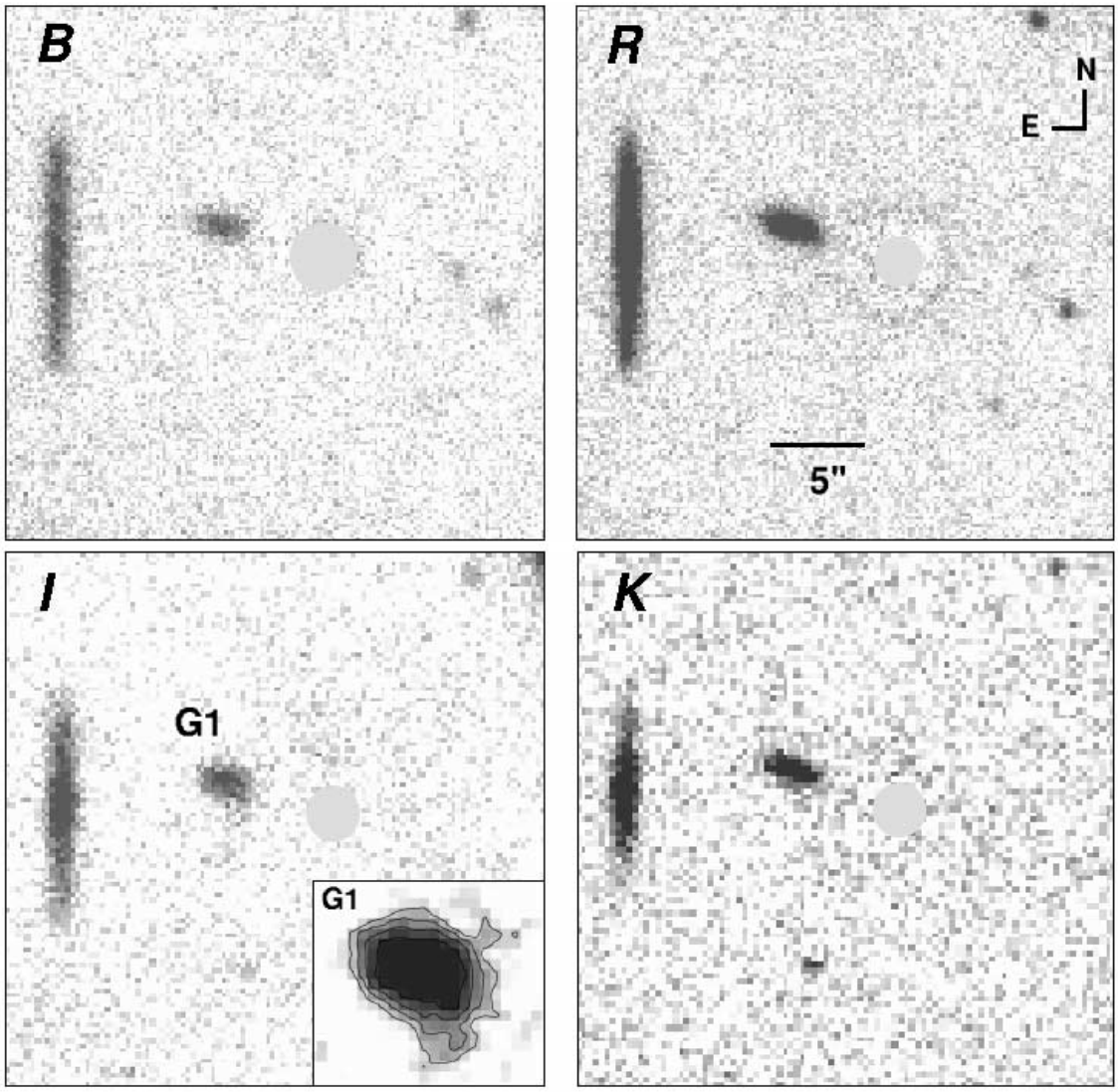

FIG. 1.—B, R, I, and K images of the B2 0827+243 field that contains a DLA system at $z = 0.525$. Quasar PSFs have been subtracted, and the residuals have been masked. G1 has a measured redshift of $z = 0.5258$ (Steidel et al. 2002) and is identified as the DLA galaxy. The inset is a smoothed image of G1 in I, where a Gaussian smoothing with $\sigma = 0.8$ pixels has been applied. The outermost contour is 1 σ above the sky background. Note that the north-south–oriented edge-on galaxy $\approx 15''$ east of the quasar is at $z = 0.199$ (Steidel et al. 2002).

LSB feature of the interacting system and was not detected in the *HST* image. In either case, the imaging data are consistent with G1 being a disturbed spiral galaxy. Steidel et al. (2002) also present Keck spectra showing the kinematic properties of G1 and of the $z = 0.525$ Mg II absorption-line system. They note that the satellite galaxy might be responsible for the apparent reversal in the direction of the radial velocity profile of G1 seen at the west end. This interaction might also be dispersing the gas out to large galactocentric radii, leading to the high H I column density of the absorbing gas and to the ≈ 270 km s^{-1} wide, four-component, Mg II absorption line. The unsaturated Mg I $\lambda 2852$ line shows similar structure, with the central two components that are ≈ 50 km s^{-1} apart being the strongest. The 21 cm absorption line has been measured at moderate spectral resolution and covers ≈ 50 km s^{-1}, although it is uncertain how many absorbing components might be contributing to the profile (Kanekar & Chengalur 2001a). Based on a comparison of redshift and velocity spread, it is likely that the H I absorption arises in gas associated with the two main Mg I absorbing clouds. Indeed, there is compelling evidence that strong Mg II absorbers that show 21 cm absorption are also associated with strong Mg I absorption (Lane 2000). Moreover, systems with larger Mg I $\lambda 2852$ rest equivalent width (or velocity spread when observed at high resolution) also have larger 21 cm line velocity spreads (Lane 2000).

Although the impact parameter of G1 is large ($b = 34$ kpc), its high inclination angle should increase the likelihood that DLA column densities could be observed at large galactocentric distances. But it is also possible that an object hidden under the quasar PSF might be the actual absorber. To explore this possibility, we subtracted the quasar PSF in the WFPC2 image, using the procedure described in Hamilton, Casertano, & Turnshek (2002), but found no convincing evidence for a galaxy hidden under the quasar PSF.

3.1.1. *Photometry of G1*

Photometric measurements of G1, along with 1 σ uncertainties, are given in Table 3. Results from stellar

TABLE 3
OBJECT PHOTOMETRY

Field	Object	$\Delta\alpha$ (arcsec)	$\Delta\delta$ (arcsec)	m_U (mag)	m_B (mag)	m_R (mag)	m_I (mag)	m_J (mag)	m_K (mag)
B2 0827+243.....	G1	+5.8	+1.9	22.61 (0.16)	22.76 (0.04)	20.82 (0.05)	20.34 (0.05)	...	17.07 (0.05)
PKS 0952+179.....	1	+2.9	−0.1	...	...	...	...	22.3 (0.2)	21.2 (0.3)
	2	−1.4	−1.8	...	...	...	...	23.1 (0.4)	20.8 (0.1)
	3	+3.7	−4.3	...	25.9 (0.3)	25.2 (0.2)	...	22.5 (0.3)	20.7 (0.2)
	4	−3.5	+5.1	...	25.0 (0.2)	24.5 (0.2)	...	22.1 (0.2)	20.1 (0.2)
	5	+6.7	−4.4	...	24.8 (0.2)	24.0 (0.1)	...	23.2 (0.4)	20.4 (0.2)
	6	−6.8	+0.5	...	27.1 (0.7)	27.1 (0.8)	...	22.3 (0.3)	20.6 (0.2)
	7	−7.5	−2.0	...	...	25.9 (0.3)	...	22.0 (0.3)	19.4 (0.1)
	8	−7.0	−3.9	...	27.9 (1.6)	25.1 (0.2)	...	23.0 (0.4)	21.8 (0.4)
	9	−1.9	+8.4	...	24.9 (0.2)	24.5 (0.1)	...	22.4 (0.3)	21.0 (0.2)
	10	−7.8	−8.7	...	25.0 (0.2)	24.5 (0.2)	...	22.5 (0.3)	21.2 (0.3)
PKS 1127−145.....	1	−3.8	+0.3	23.00 (0.19)	24.09 (0.15)	22.58 (0.08)	...	21.87 (0.13)	20.64 (0.15)
	2	−2.5	−5.8	>23.9	>24.8	>24.5	...	22.02 (0.13)	>20.3
	3	+5.4	−1.6	23.55 (0.21)	23.68 (0.09)	22.40 (0.07)	...	20.94 (0.07)	20.23 (0.20)
	4	−3.2	+7.2	23.93 (0.25)	24.94 (0.17)	24.11 (0.19)	...	22.93 (0.22)	20.96 (0.30)
PKS 1629+120.....	G1	+0.8	−2.9	22.61 (0.09)	23.15 (0.11)	21.37 (0.04)	...	19.20 (0.07)	17.65 (0.06)

NOTE.—Numbers in parentheses are 1 σ errors.

population spectral evolutionary synthesis model fits redshifted to $z = 0.525$ are shown in Figure 2. Details of the models and fitting procedures are described in the Appendix. The best-fit single-burst model, a 0.05 Gyr old burst with $E(B-V) = 0.6$, results in a reduced χ^2 of 5.5. A family of two-burst models having approximately equal combinations by mass of (1) a dusty [$0.6 \lesssim E(B-V) \lesssim 0.9$], young (0.01 Gyr) burst and (2) a nearly dust-free [$0.0 \lesssim E(B-V) \lesssim 0.2$], 0.2–0.6 Gyr old burst have the smallest reduced χ^2 values, but these are also statistically poor fits, with reduced χ^2 values between 4.8 and 5.2. The fit with the smallest reduced χ^2 is shown in Figure 2. Apparent magnitudes from Table 3, along with K-corrections derived from this best-fit model, give absolute magnitudes for G1 of $M_U = -20.3$, $M_B = -20.6$, $M_R = -21.7$, $M_I = -22.1$, and $M_K = -24.7$ at $z = 0.525$.

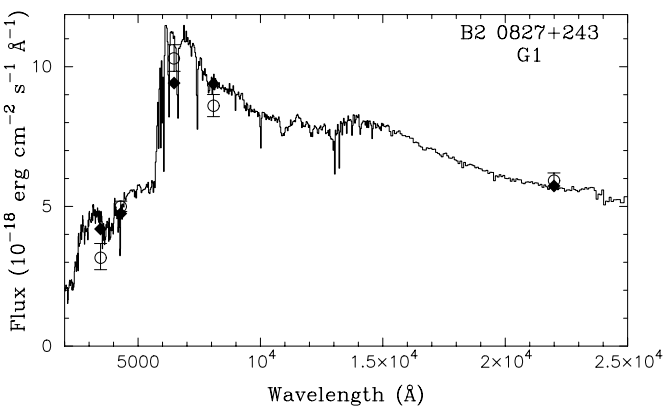

FIG. 2.—Best-fit two-burst model of a galaxy at $z = 0.525$, overlaid on the photometry of G1 in the B2 0827+243 field. The circles with 1 σ error bars represent photometric measurements. For comparison, the diamonds represent model flux values determined at the effective wavelength of the filter by convolving the filter response function with the model spectral energy distribution. The model is a two-burst combination of (1) a 48% by mass burst that is young (0.01 Gyr) and dusty, with $E(B-V) = 0.6$, and (2) a 52% by mass burst that is older (0.6 Gyr) and dust-free, with $E(B-V) = 0.0$.

3.2. *PKS 0952+179*

The DLA system toward this quasar is at redshift $z = 0.239$, with column density $N_{\rm HI} = (2.1 \pm 0.3) \times 10^{21}$ atoms cm^{-2} (RT2000). Figure 3 shows $20'' \times 20''$ images of this field through the B, R, J, and K filters. The quasar PSF has been subtracted in the B, R, and J images, and the residuals have been masked out. The quasar has simply been masked out in the K-band image, because there were no suitable bright stars in the IRTF-NSFCAM field of view that could be used to perform a good PSF subtraction of the quasar light. All four images have been smoothed to enhance LSB features. Objects identified in the J image that are detected in at least one of the B, R, and K images have been numbered sequentially in order of increasing radial distance from the quasar. The objects labeled 1 and 2 are detected in both J and K and, because of their proximity to the quasar sight line, are our best candidates for the DLA galaxy. Their morphology suggests that they might be two nearly edge-on galaxies. While the J image, with a seeing of $0''.7$ and limiting surface brightness of 24 mag arcsec^{-2}, is exceptionally good by ground-based imaging standards, higher resolution imaging, for example with NICMOS on *HST*, is required to be better able to resolve these features and, perhaps, comment on the nature of the $z = 1.478$ quasar host galaxy as well (see Kukula et al. 2001). Table 3 gives the positions of the labeled objects relative to the quasar, along with apparent magnitudes and 1 σ uncertainties.

3.2.1. *An ERO at $z = 0.239$?*

The brightest of these in K, object 7, is an extremely red object (ERO), with $R-K = 6.5$ (see Table 3). EROs are generally thought to be either elliptical galaxies at $z \gtrsim 1$ whose red colors are due to large K-corrections or star-forming galaxies whose red colors are due to heavily obscured stellar or AGN emission (see, e.g., Cimatti et al. 1999; Dey et al. 1999; Daddi, Cimatti, & Renzini 2000; Smith et al. 2001). The lowest redshift ERO known is the $z = 0.65$ galaxy PDF J011423 (Afonso et al. 2001), whose red colors and spectral energy distribution (SED) are consistent with its being a dusty starburst with 5–6 mag of optical extinction. Other

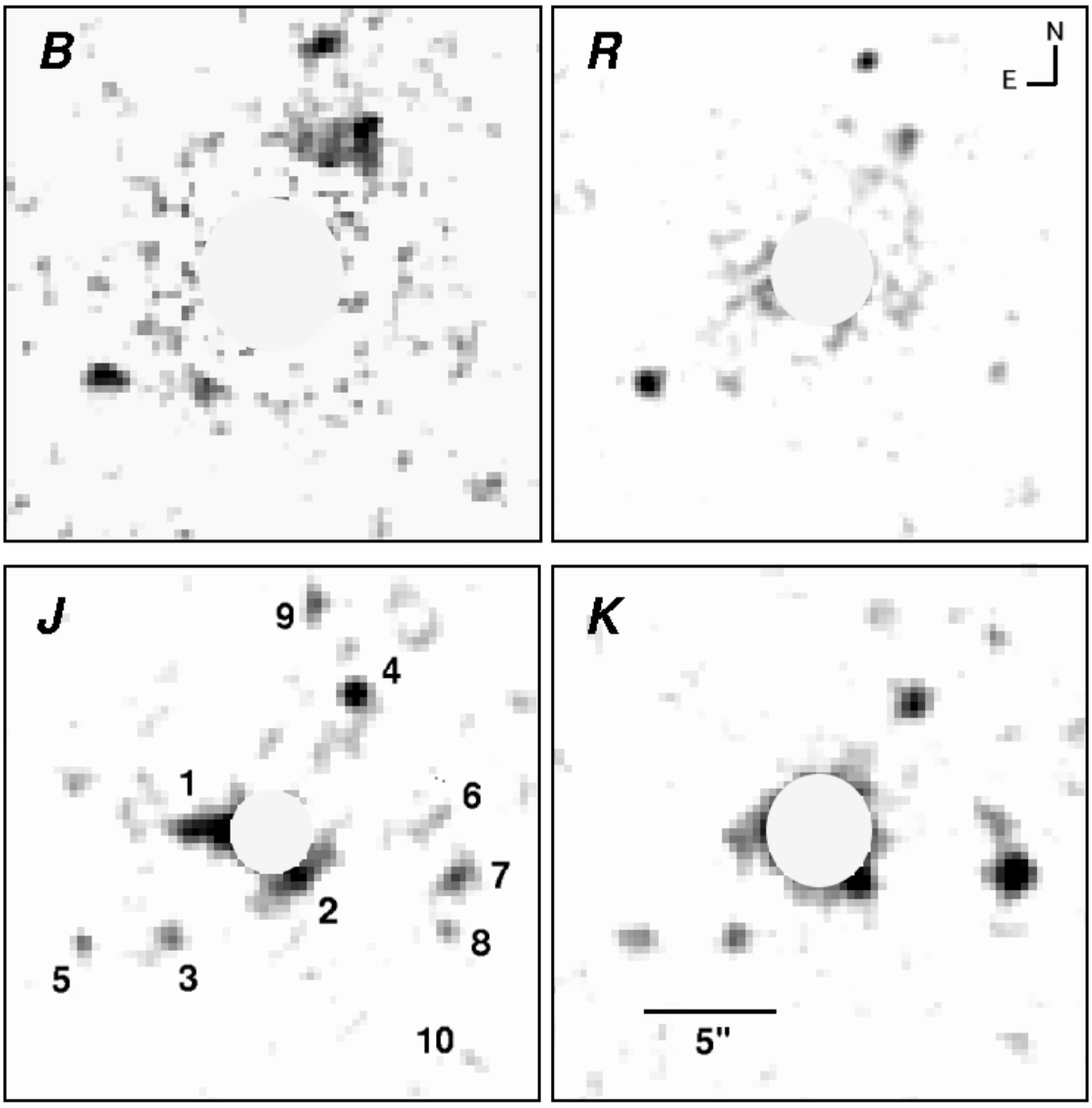

FIG. 3.—Smoothed B, R, J, and K images of the PKS 0952+179 field that contains a DLA system at $z = 0.239$. The PSF of the quasar has been subtracted in the B, R, and J images, but not in the K image, as there was no suitable PSF star in the field. The residuals in B, R, and J and the quasar in K have been masked. Objects are labeled only on the J image, for clarity. All 10 of these are detected in K. Features in the B and R images that lie at the edges of the mask are artifacts of the PSF subtraction process; only objects labeled 3, 4, 5, 8, 9, and 10 are detected in B, while those labeled 3, 4, 5, 7, 8, 9, and 10 are detected in R. Objects 1 and 2 are the best candidates for the DLA galaxy. Object 7 is an ERO, with $R-K = 6.5$. See § 3.2 for more details.

EROs classified as starbursts have similar dust extinctions (Afonso et al. 2001). PDF J011423 is bright in K ($m_K = 15.3$) and has extremely red colors, with $R-K = 5.8$ and $J-K = 3.1$. In comparison, object 7 is relatively faint, with $K = 19.4$, and is also extremely red, with $R-K = 6.5$ and $J-K = 2.6$. The redshift of object 7 is not known, but if it is at the DLA redshift, it would have to be a star-forming region that is heavily obscured by dust. At $z = 0.239$, $K = 19.4$ corresponds to $M_K = -20.7$, where a K-band K-correction of -0.2 mag has been applied (Cowie et al. 1994). This implies an absolute luminosity of $L_K = 0.03L_K^*$, comparable to the luminosity of a single star-forming region within a galaxy. We find that, based on G. Bruzual A & S. Charlot (2003, in preparation) GISSEL99 galaxy spectral evolutionary synthesis models, its colors can be attributed to a region of star formation with age $\lesssim 0.6$ Gyr at $z = 0.239$, if the extinction is $A_V \gtrsim 4.8$. Thus, the luminosity, colors, and implied extinction are consistent with object 7 being at $z = 0.239$. If confirmed, it would be the lowest redshift ERO known.

However, the observational constraints are not tight enough to rule out the possibility that object 7 is a higher redshift elliptical galaxy. Its colors fall on the "starburst" side, but near the edge, of the $R-K$ versus $J-K$ plane used to classify EROs (Pozzetti & Mannucci 2000). Uncertainties in our photometry, as well as in the definition of the plane, do not preclude object 7 from crossing the plane and being classified as a passively evolving elliptical galaxy at $z \approx 1.5$ (Cimatti et al. 1999). In this case, object 7 might be part of a cluster of galaxies that also includes the quasar PKS 0952+179 ($z_{em} = 1.478$); it would be $\sim L^*$ at this redshift. We detect a significant number of EROs in the extended $5' \times 5'$ field surrounding this quasar (D. B. Nestor et al. 2003, in preparation), and this might be supporting evidence for the overdensity of EROs found by Cimatti et al. (2000) around

radio-loud quasars. Thus, the proximity of object 7 to the DLA galaxy might just be a coincidence.

3.2.2. *The DLA Galaxy*

While the nature of none of the objects labeled in Figure 3 is known for certain, it is of interest to examine the possibility that they are star-forming regions associated with the DLA galaxy. The colors of all the labeled features are consistent with their being at $z = 0.239$, but with varying degrees of obscuration. The implications might be that the DLA galaxy is either a patchy LSB galaxy or a disturbed system in which object 7 is a recently triggered star-forming region. The galaxy would extend anywhere from $\approx$45 (objects 1–7) to $\approx$55 kpc (objects 5–7). The total luminosity of the PKS 0952+179 DLA galaxy cannot be measured, since some of it is likely to be hidden by the quasar PSF. The total luminosity of all the objects labeled in Figure 3 is $m_K = 18.1$. If this is considered a lower limit to the luminosity of the DLA galaxy, then $M_K < -22.0$, or $L_K > 0.1L_K^*$. If only objects 1 and 2 were part of the DLA galaxy, it would extend $\approx$24 kpc, with $m_K < 20.2$, $M_K < -19.5$, and $L_K > 0.01L_K^*$. If objects 1 and 2 were two edge-on galaxies, as their *J*-band morphologies might suggest, then possibly half of the galaxy that is object 1 is obscured by the quasar PSF. In this case, each of the edge-on galaxies would be a dwarf with a luminosity on the order of $0.01L_K^*$.

However, in the absence of higher resolution imaging, we tentatively identify the DLA galaxy as objects 1 and 2, since these have the smallest impact parameters, and since there is no observable emission between these and objects 3–10. Given the assumption that half of object 1 is obscured by the quasar PSF, objects 1 and 2 have a total luminosity of $L_K = 0.02L_K^*$. Since these objects extend into the quasar PSF, their impact parameter cannot be determined to better than the radius of the circle that encloses all residuals left over from subtracting the quasar PSF in the unsmoothed *J*-band image. This is because subtracting the PSF resulted in noisy residuals near the PSF core, and no useful information could be extracted within this radius. The radius was measured to be $1\farcs2$, which, at $z = 0.239$, implies $b < 4.5$ kpc.

We note that luminous galaxies in the extended field surrounding this quasar have spectroscopic redshifts different from the DLA absorption redshift (Bergeron & Boissé 1991) and that the $z = 0.239$ system is the only known absorption-line system in the spectrum of this quasar. High-resolution observations of the $z = 0.239$ Mg II absorption line do not exist, and so the kinematic structure of the Mg II–absorbing gas has not been studied in detail. However, the 21 cm absorption line is narrow, with an FWHM of only 7.7 km s^{-1} (Kanekar & Chengalur 2001a), indicative of simple kinematic structure.

3.3. *PKS 1127−145*

This DLA system is at $z = 0.313$, with column density $N_{\rm HI} = (5.1 \pm 0.9) \times 10^{21}$ atoms cm^{-2} (RT2000). Figure 4 shows $\approx 50'' \times 50''$ images of this field in *U*, *B*, *R*, and *J*. The quasar PSF has been subtracted in each of the four images, and the residuals have been masked out. Furthermore, the images have been smoothed to enhance LSB features. The two large spiral galaxies, labeled "a" and "b," are at the DLA redshift (Bergeron & Boissé 1991). Galaxy a is clearly warped and has a dwarf companion $\approx 2''$ to the southwest. Galaxy b has a faint extension toward the east that is visible in *R* and *J*. The object $3''$ west of the quasar, labeled "1," is an emission-line object with a confirmed redshift of $z = 0.3121 \pm 0.0003$ (Lane et al. 1998). No emission lines were detected in the spectrum of object 3, and so its redshift is not known. However, the *J*-band image in Figure 4 suggests that there may be LSB features to the east of the quasar that extend out to the position of object 3. Thus, we identify the DLA galaxy as the patchy/irregular LSB structure visible primarily in *J* that extends $\approx 10''$ (44 kpc) in the north-south, as well as the east-west, direction and encompasses objects 1, 2, 3, and 4.[2]

Since the DLA galaxy as defined above overlaps with the quasar PSF, its impact parameter cannot be determined to better than the radius of the circle that encloses all residuals left over from subtracting the quasar PSF in the unsmoothed *J*-band image. This radius, which we assume is an upper limit to the DLA galaxy's impact parameter, was measured to be $1\farcs5$, which, at $z = 0.313$, implies $b < 6.5$ kpc. No useful information could be extracted within this radius. The DLA galaxy is quite possibly the remains of a dwarf galaxy (see § 3.3.1) that is being tidally disrupted by the more massive spiral galaxies and in which these four objects represent regions of recent star formation.

3.3.1. *Photometry*

Photometric measurements of objects 1–4 are given in Table 3, along with their 1 σ uncertainties. Object 2 is below the detection limit in *R* and has $R-J > 2.3$. Lower limits to the *U*, *B*, *R*, and *K* magnitudes of object 2 were measured with the same aperture size used to measure its magnitude in *J*.

Objects 1, 3, and 4 have blue colors. Stellar population synthesis model fits to the photometry of these star-forming regions are shown in Figure 5. Details of the models are given in the Appendix. For object 1, a family of single bursts fits the data well. These have burst ages ranging from 0.1 to 0.3 Gyr and $0.0 \lesssim E(B-V) \lesssim 0.10$. The top panel of Figure 5 shows the best-fit model, which is a 0.2 Gyr old burst with no extinction. This fit resulted in a reduced χ^2 of 1.37.

Single-burst models are not a good fit to the photometry of object 3. The best fit has a high reduced χ^2 of 3.80. For two-burst models the best fit, with a reduced χ^2 of 1.77, is obtained when the populations are (1) an $\approx$70% by mass burst that is young (0.001 Gyr) and dusty, with $E(B-V) \approx 0.7$, and (2) an $\approx$30% by mass burst that is 1.0 Gyr old with no dust. This two-burst model is shown in the middle panel of Figure 5.

Object 4 is well fitted by a family of single bursts having ages in the range of 0.01–0.05 Gyr and $0.05 \lesssim E(B-V) \lesssim 0.2$. Of these, the best-fit model is a 0.01 Gyr burst with $E(B-V) = 0.2$ and results in a reduced χ^2 of 1.01. This single-burst model is shown in the bottom panel of Figure 5.

The absolute magnitudes of the three objects were determined using the apparent magnitudes given in Table 3, along with *K*-corrections derived from their best-fit SED. In the *R* band, these are −18.1, −18.6, and −16.6 for objects 1, 3, and 4, respectively, giving a total *R*-band luminosity for

[2] We note that objects in this field were discussed in Lane (2000), where galaxies a and b were labeled G1 and G2 and objects 1 and 3 were labeled G3 and G4, respectively.

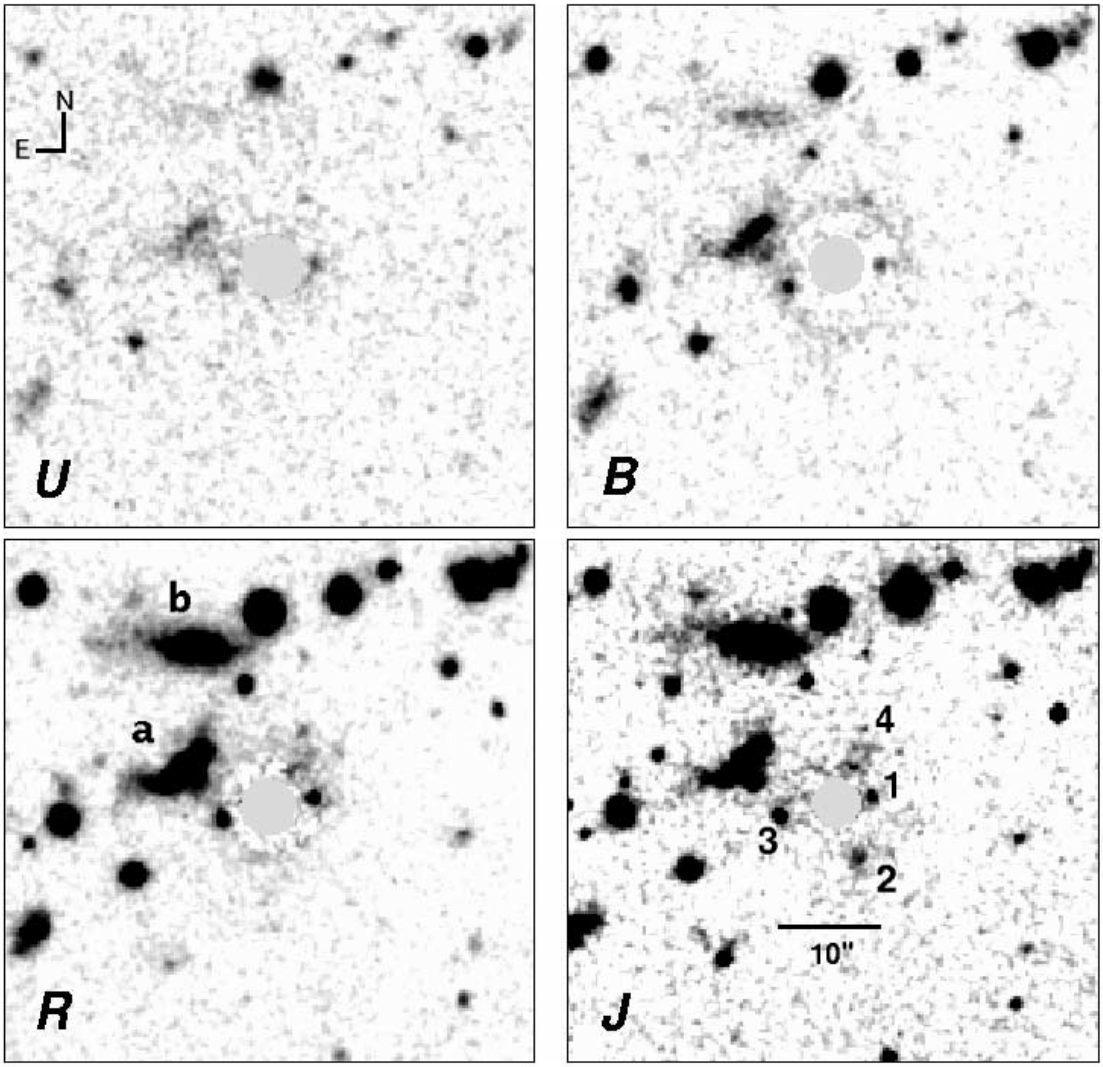

FIG. 4.—Smoothed U, B, R, and J images of the PKS 1127−145 field that contains a DLA system at $z = 0.313$. The PSFs of the quasar have been subtracted and the residuals masked. The DLA galaxy is assumed to be the patchy/LSB structure that extends between objects 3 and 1 in the east-west direction and between objects 4 and 2 in the north-south direction. Object 1 has a measured slit redshift of $z = 0.3121$. The two large spiral galaxies in the field, labeled "a" and "b," are also at the DLA redshift. Note the presence of several EROs that are visible in J but are faint or below the detection limit in R. The ringlike structures around the quasar in B and R, left over from the quasar PSF subtraction process, appear enhanced because of the smoothing and are not real.

the galaxy of $M_R = -19.2$, or $L_R = 0.16L_R^*$. Here, we have added the luminosities of the three features and reported the result as the luminosity of the DLA galaxy. In the K band, we find absolute magnitudes −19.7, −20.2, and −19.6, with a total K-band luminosity of $M_K^* = -21.0$, or $L_K = 0.04L_K^*$.

3.3.2. *More EROs*

Closer inspection of Figure 4 reveals many objects in this $50'' \times 50''$ field that are relatively bright in J but are below the detection limits or are very faint in R. Several of these are in the vicinity of galaxy b and could well be dusty regions in which star formation is being triggered by the interaction between galaxies a and b. Their location is compelling evidence for their association with the $z = 0.313$ galaxies, although the possibility that they are associated with the radio-loud, $z_{\rm em} = 1.187$ quasar cannot be ruled out.

3.3.3. *Kinematics*

High-resolution observations of the Mg II absorption line have not been published, but the high rest equivalent width of the 2796 Å line, $W_0^{\lambda 2796} = 2.21$ Å, implies a velocity width of $\gtrsim 240$ km s^{-1}. The 21 cm absorption-line profile of this DLA system is also complex (Lane 2000), and it has been shown to vary on timescales of a few days (Kanekar & Chengalur 2001b). The 21 cm absorption line extends over 85 km s^{-1} and is resolved into five components. The deepest component, with optical depth $\tau \approx 0.11$, is at the low-velocity end of the profile. Prochaska & Wolfe (1997, 1998) have used simulations to show that this type of leading-edge profile is produced along a line of sight that passes through a rotating disk. On the other hand, Haehnelt, Steinmetz, & Rauch (1998), who consider gas infall due to merging, and McDonald & Miralda-Escudé (1999), who consider moving clouds in a spherical halo, have also reproduced leading-edge line profiles. In the case of the PKS 1127−145 DLA system, both the image and kinematics are more consistent with the latter interpretations. However, this DLA system appears to be even more complex in its structure and kinematics, since it is not an isolated system and probably owes its morphology to the nature of its environment.

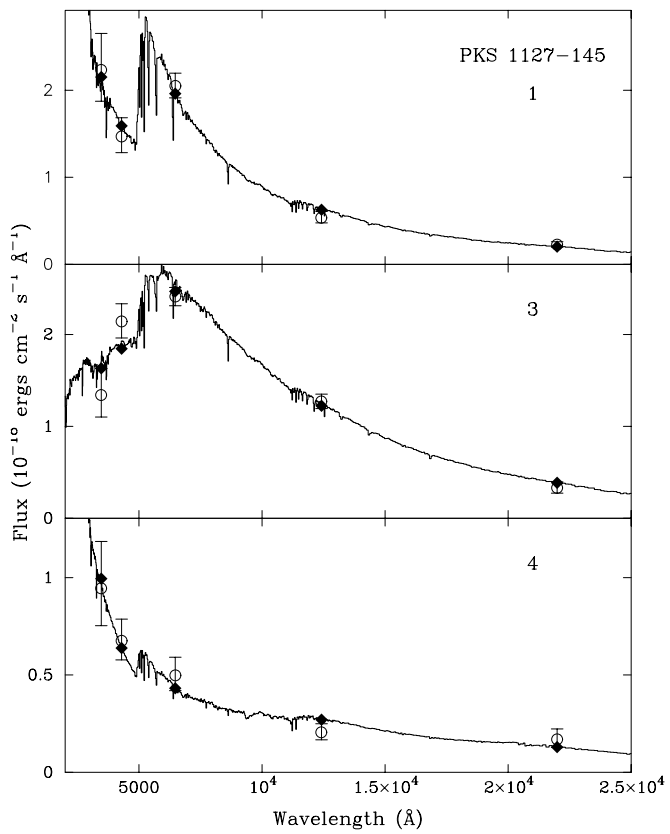

FIG. 5.—Stellar population spectral synthesis model fits at $z = 0.313$ for objects 1, 3, and 4 in the PKS 1127−145 field. Symbols are as in Fig. 2. The best-fit model for object 1 is a single 0.2 Gyr old burst with no extinction. Object 3 is best fitted by a two-burst model with (1) an ≈70% by mass burst that is young (0.001 Gyr) and dusty, with $E(B-V) \approx 0.7$, and (2) an ≈30% by mass burst that is 1.0 Gyr old with no dust. Object 4 is best fitted by a single 0.01 Gyr burst with $E(B-V) = 0.2$.

3.4. *PKS 1629+120*

The sight line toward the quasar PKS 1629+120 ($V = 18.4$, $z_{em} = 1.795$) contains a DLA system at $z = 0.532$, with column density $N_{HI} = (5.0 \pm 1.0) \times 10^{20}$ atoms cm^{-2}. We discovered this system in an *HST* Cycle 9 survey for DLA lines in strong Mg II–Fe II absorption-line systems.

3.4.1. *The UV Spectrum*

Figure 6 shows the *HST*-STIS G230L NUV-MAMA spectrum, while Figure 7 shows a Voigt profile with column density $N_{HI} = 5.0 \times 10^{20}$ atoms cm^{-2} overlaid on the DLA line. The error in the column density estimate is dominated by the uncertainty in continuum placement and was determined using a procedure similar to that described in RT2000. This line of sight has two Mg II systems, one at $z = 0.5313$ with Mg II $W_0^{\lambda 2796} = 1.40$ Å and Fe II $W_0^{\lambda 2600} = 0.70$ Å (Aldcroft et al. 1994), and one at $z = 0.9005$ with Mg II $W_0^{\lambda 2796} = 1.06$ Å and Fe II $W_0^{\lambda 2600} = 0.63$ Å (Barthel, Tytler, & Thomson 1990). The $z = 0.9005$ system is sub-DLA, with $N_{HI} = (5.0 \pm 0.4) \times 10^{19}$ atoms cm^{-2}. We also detect a Lyα line at 2895 Å, with rest equivalent width $W_0^{\lambda 1216} = 1.4$ Å, that is associated with a C IV system at $z = 1.3786$ (Aldcroft et al. 1994). The strongest line in the blend at 2952 Å has $W_0^{\lambda 1216} = 2.5$ Å; it has no known associated metal line absorption.

3.4.2. *Imaging Results*

Figure 8 shows ≈40″ × 40″ *U*, *B*, *R*, and *K* images of this field. All four quasar PSFs have been subtracted, resulting in residuals that are comparable to the background in each image. The position of the quasar is marked with a plus sign. Unresolved objects are labeled with an "S" and are presumed to be stars, while resolved objects are galaxies labeled with a "G." They are numbered in order of increasing distance from the quasar. G1 appears patchy in *U*, possibly indicating regions of recent star formation. An edge-on, disklike structure can be seen in *B*. It appears bulgelike in *K* and shows signs of both bulge and disk structure in *R*. These morphological features are consistent with G1 being a mid-type spiral galaxy. As we show below, the photometry of G1 is consistent with it being the DLA galaxy at $z = 0.532$. In this case, its impact parameter, i.e., the projected distance from the center of G1 to the center of the PSF of the quasar, is $b = 17$ kpc.

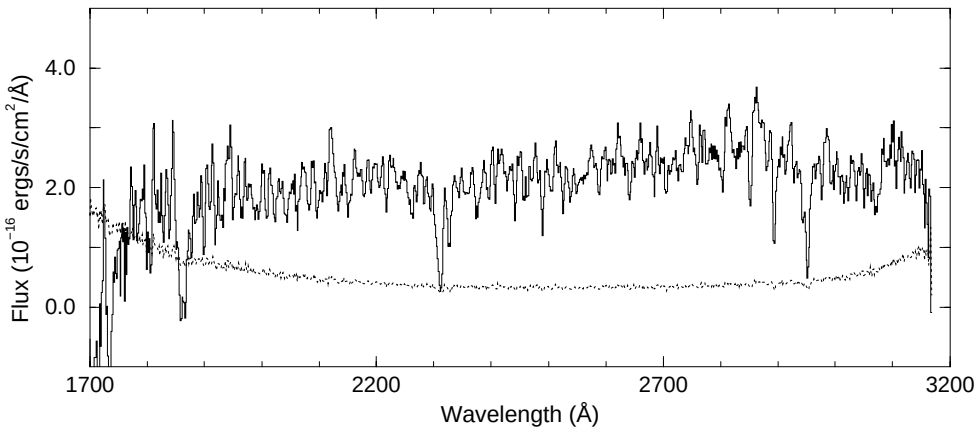

FIG. 6.—*HST*-STIS spectrum of PKS 1629+120. The 1 σ error spectrum is also shown. Both of the Mg II lines along this line of sight are associated with strong Lyα absorption. The absorption feature at 1863 Å is a DLA line at $z = 0.532$ with $N_{HI} = (5.0 \pm 1.0) \times 10^{20}$ atoms cm^{-2} (see Fig. 7), and the absorption line at 2306 Å is sub-DLA at $z = 0.901$ with $N_{HI} = (5.0 \pm 0.4) \times 10^{19}$ atoms cm^{-2}. The Lyα line at 2895 Å has rest equivalent width $W_0^{\lambda 1216} = 1.4$ Å and is associated with a C IV system at $z = 1.3786$ (Aldcroft, Bechtold, & Elvis 1994). The strongest line in the blend at 2952 Å has $W_0^{\lambda 1216} = 2.5$ Å; it has no known associated metal line absorption.

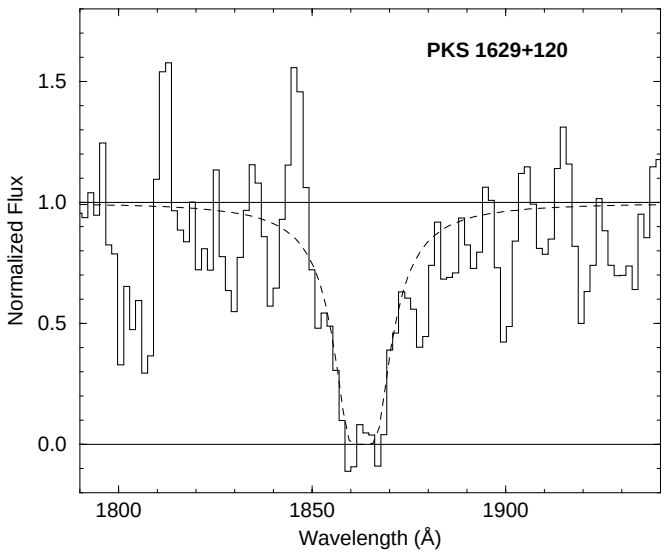

FIG. 7.—Portion of the *HST*-STIS spectrum of PKS 1629+120, showing the DLA line at $z = 0.532$. The overlaid Voigt profile has $N_{\rm HI} = 5.0 \times 10^{20}$ atoms cm^{-2}.

3.4.3. *Photometry of G1*

Photometric measurements and 1 σ uncertainties of G1 are given in Table 3. These magnitudes were used to determine a photometric redshift for G1 by using the galaxy spectral templates of G. Bruzual A & S. Charlot (2003, in preparation) in a principal component analysis (A. Conti 2002, private communication). The best-fit template was determined at redshifts $0 < z < 2$ in steps of 0.001. The resulting reduced χ^2, which was determined at each step, has a minimum equal to 0.7 at $z \approx 0.59$, and redshifts in the range $0.50 < z < 0.65$ are good fits, with reduced $\chi^2 \leq 1$. The reduced χ^2 at $z = 0.90$ is $\approx$4, making $z = 0.90$ approximately 30 times less probable than $z = 0.59$. Therefore, we can rule out the possibility that G1 is the sub-DLA galaxy at $z = 0.901$ (see § 3.4.4) and assume that G1 is the DLA galaxy at $z = 0.532$. However, we note that a slit redshift is required to unambiguously determine the redshift of G1.

We also fit stellar population synthesis models to the photometry, as described in the Appendix. The best-fit model, which results in a reduced $\chi^2 = 0.82$, is shown in Figure 9. It is a single, 0.05 Gyr old burst and has $E(B-V) = 0.5$. The apparent magnitudes from Table 3, in combination with K-corrections derived from this model, give absolute magnitudes of $M_U = -20.3$, $M_B = -20.3$, $M_R = -21.3$, $M_J = -23.0$, and $M_K = -23.9$ at $z = 0.532$.

3.4.4. *The $z = 0.901$ Sub-DLA Galaxy*

G1 is the only galaxy detected near the quasar sight line, and we have shown that its photometry is consistent with it being the $z = 0.532$ DLA galaxy. Having assumed that G1 is at $z = 0.532$, we must now consider the whereabouts of the $z = 0.901$ sub-DLA galaxy. One possibility is that it, too, has a small impact parameter but is below the detection limit of all our images. A second possibility is that it lies directly along the line of sight to the quasar and was subtracted along with the quasar PSF. Third, it might be one of the galaxies detected at large impact parameter. We consider each of these in turn.

If the first possibility is true, then the $z = 0.901$ galaxy must have a surface brightness of $\mu_K > 21.6$ mag arcsec^{-2} and $\mu_R > 25.4$ mag arcsec^{-2} at the 3 σ level (see Table 2). Assuming that it is a face-on galaxy with an extent of 20 kpc, we find that $m_R > 23.2$ and $M_R > -21.5$, where a K-correction for an Sb-type galaxy has been applied (Poggianti 1997), or $L_R < 1.3L_R^*$. Similarly, in the K band we find $m_K > 19.4$ and $M_K > -24.4$, or $L_K < 0.4L_K^*$.

The quasar PSF was subtracted reasonably cleanly, since the PSF was well sampled by several stars brighter than the quasar in each frame. If there is a galaxy coincident on the sky with the quasar, then it would have to mimic a point source and be centered exactly on the quasar PSF. Although this is a possibility, it is highly unlikely.

Except for G1, all detected galaxies lie between 11″ and 19″ from the quasar and have impact parameters between 72 and 124 kpc at $z = 0.901$, i.e., much larger than what is typical for Mg II absorbers (Steidel 1993). The implied impact parameters at $z = 0.532$ are also very large, ranging between 62 and 107 kpc. Therefore, from impact parameter considerations, these are not likely to be either of the two absorbing galaxies.

Finally, we note that if G1 was at $z = 0.901$, then the DLA galaxy, which would have gone undetected, would have to have $L_R < 0.3L_R^*$ and $L_K < 0.2L_K^*$. Moreover, G1 would have $L_R = 2.1L_R^*$ and $L_K = 4.5L_K^*$, and it would be an unusually luminous low-redshift sub-DLA galaxy. Thus, it is more reasonable to conclude that G1 is at $z = 0.532$ and that the $z = 0.901$ sub-DLA galaxy is not detected in our images.

4. DISCUSSION

The four new low-redshift DLA galaxies presented here have an interesting mix of morphologies. The two higher redshift galaxies, G1 B2 0827+243 ($z = 0.525$) and G1 PKS 1629+120 ($z = 0.532$) are $\approx L^*$ spirals. Higher resolution *HST* observations of the former reveal that an interaction between the luminous spiral and a satellite dwarf galaxy might be responsible for the presence of DLA gas at larger galactocentric distances. We have, a posteriori, detected an extension to G1 in our ground-based images that might indicate the presence of a satellite. In the absence of high-resolution images of the PKS 1629+120 field, we cannot offer a more detailed description of that DLA galaxy's morphology.

Images of the two lower redshift DLA systems are more complex. Lacking higher resolution images, there are two possible identifications for the $z = 0.239$ PKS 0952+179 DLA galaxy. Either it is the object(s) that overlaps with the QSO PSF in the J-band image, or it is a larger, irregular dwarf galaxy with patchy structure. In the former case, it is unlikely that the luminosity of this DLA galaxy exceeds a few hundredths of L^*. Faint, patchy morphology is also present in the $z = 0.313$ DLA galaxy in the PKS 1127−145 field. However, in this case numerous star-forming regions are clearly visible. These regions are blue and displaced enough from the quasar sight line that a confirming slit redshift has been obtained for one of them. Because of the appearance of this patchy, irregular structure, it is likely that the nearby $\approx L^*$ spiral galaxies, the closer one of which was once thought to be the DLA galaxy, are responsible for tidally disrupting the actual DLA galaxy that lies along the line of sight to the quasar. Thus, the DLA galaxy takes the

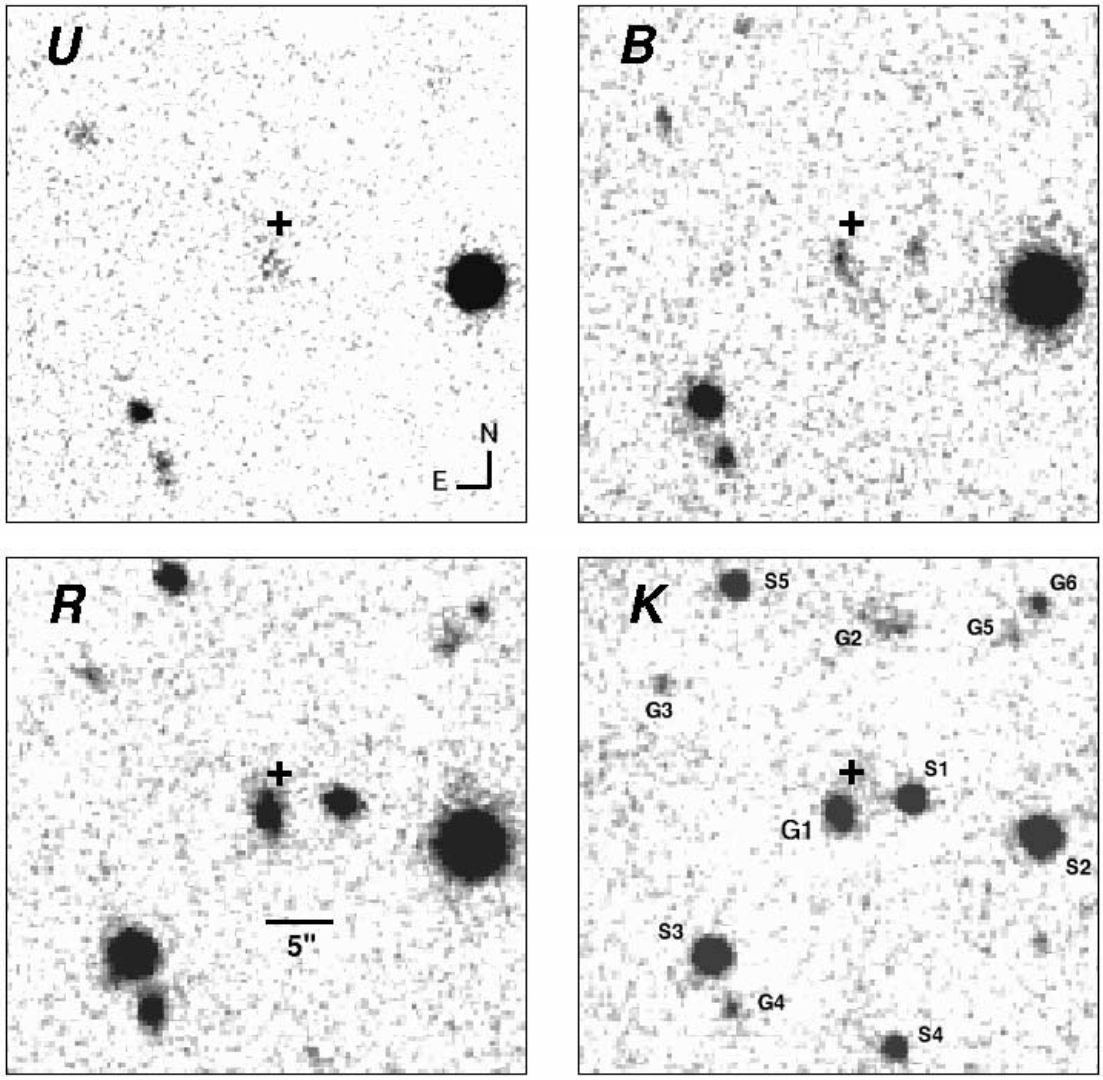

FIG. 8.—*U*, *B*, *R*, and *K* images of the PKS 1629+120 field that contains a DLA system at $z = 0.532$. The PSF of the quasar, whose position is marked with a plus sign, has been subtracted in all four images. The PSF subtraction here is cleaner than in the other three DLA fields, since PKS 1629+120 is relatively faint. Resolved objects are labeled with a "G," and unresolved objects are labeled with an "S." G1 is identified as the DLA galaxy.

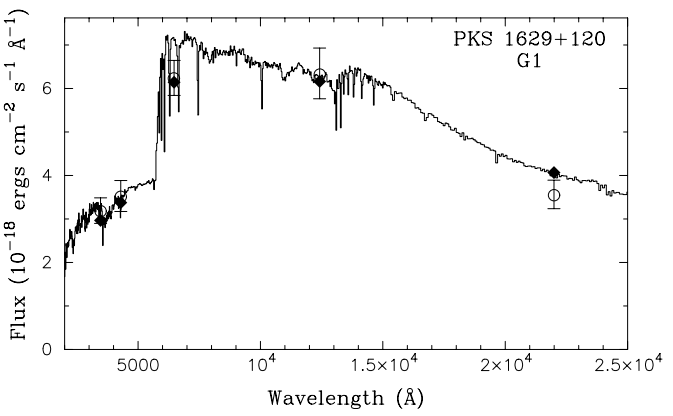

FIG. 9.—Best-fit single-burst model at $z = 0.532$, overlaid on the photometry for G1 in the PKS 1629+120 field. Symbols are as in Fig. 2. The model is a 0.05 Gyr old single burst with $E(B-V) = 0.5$.

form of an extended irregular structure with star-forming regions. However, the possibility that these star-forming regions are individual interacting or merging galaxies cannot be ruled out. Again, higher resolution images would be needed to clarify the situation. Whichever is the case, the total light from the DLA galaxy does not exceed $0.16L^*$.

These observations add to the small but growing list of DLA galaxies at low redshifts. Table 4 lists the status and properties (luminosity relative to L^*, L/L^*, neutral hydrogen column density, $N_{\rm HI}$, and impact parameter, b) of galaxy identifications for 14 DLA systems with $z_{\rm DLA} \lesssim 1$ and $N_{\rm HI} \geq 2 \times 10^{20}$ atoms cm^{-2} (but not including local galaxies). The distributions of DLA galaxy properties for these 14 cases are shown in Figure 10. *B*-band luminosities are plotted when available. *K*-band luminosities are plotted for galaxies that are not detected in *B*, but this substitution should not grossly affect any trends in the data. For the case of the DLA galaxy in the 3C 336 field, only an upper limit to its luminosity can be determined, since the galaxy is not detected. For the same reason, the impact parameter is unknown. This case is clearly representative of another

TABLE 4
LOW-REDSHIFT DLA GALAXY PROPERTIES

QSO	z_{DLA}	$N_{HI}/10^{20}$ (atoms cm^{-2})	Luminosity[a]	b (kpc)	Morphology	Reference
This Work						
B2 0827+243	0.525	2.0	$0.8L_B^*$, $1.6L_R^*$, $1.2L_K^*$	34	Disturbed spiral	1
PKS 0952+179	0.239	21	$0.02L_K^*$[b]	<4.5	Dwarf LSB	1
PKS 1127−145	0.313	51	$0.12L_B^*$, $0.16L_R^*$, $0.04L_K^*$[c]	<6.5	Patchy/irr/LSB	1
PKS 1629+120	0.532	5.0	$0.6L_B^*$, $1.1L_R^*$, $0.6L_K^*$	17	Spiral	1
Other Work						
AO 0235+164	0.524	45[e]	$0.8L_B^*$	6.0	Late-type spiral[e]	2, 3
EX 0302−223	1.010	2.3	$0.2L_B^*$	9.2	Semicompact	4
PKS 0454+039	0.859	4.7	$0.4L_B^*$	6.4	Compact	4
Q0738+313 (OI 363)	0.091	15	$0.08L_K^*$	<3.6	LSB	5
	0.221	7.9	$0.1L_B^*$	20	Dwarf spiral	5
Q0809+483 (3C 196)	0.437	6.3	$1.7L_B^*$	9.6	Giant Sbc	4
Q1209+107	0.633	2.0	$1.6L_B^*$	11.2	Spiral	4
PKS 1229−021	0.395	5.6	$0.1L_B^*$	7.6	LSB	4, 6
Q1328+307 (3C 286)	0.692	15	$0.4L_B^*$	6.5	LSB	4, 6
Q1622+239 (3C 336)	0.656	2.3	$<0.05L_K^*$	...	LSB? compact?	7

NOTE.—Only galaxies with cosmological redshifts are included. Thus, the DLA galaxy at $z = 0.010$, SBS 1543+593, is excluded, since it does not fall well beyond the local velocity field, which is defined at 3000 km s^{-1} by the outer boundary of the Virgo cluster (Binggeli, Popescu, & Tammann 1993). We note that it is an LSB galaxy, with $L_B = 0.02L_B^*$ and $b = 0.8$ kpc (Bowen, Tripp, & Jenkins 2001; R. E. Schulte-Ladbeck et al. 2003, in preparation).

[a] $M_B^* = -20.9$ (Marinoni et al. 1999), $M_R^* = -21.2$ (Lin et al. 1996), and $M_K^* = -24.5$ (Loveday 2000), for $q_0 = 0.5$ and $H_0 = 65$ km s^{-1} Mpc^{-1}.

[b] Sum of luminosities of objects 1 and 2 (see § 3.2.2 and Fig. 3).

[c] Sum of luminosities of objects 1, 3, and 4 (see § 3.3.1 and Fig. 4).

[d] Column density from Turnshek et al. 2003.

[e] The object defined as A1 in Yanny, York, & Gallagher 1989 and Burbidge et al. 1996 has the smallest impact parameter and, therefore, we have assumed that it is the DLA galaxy. A K-correction of 1 mag, which is appropriate for a late-type spiral galaxy at $z = 0.524$ (Poggianti 1997) has been applied to derive the absolute luminosity of A1 from the apparent magnitude measured by Burbidge et al. 1996.

REFERENCES.—(1) This paper. (2) Burbidge et al. 1996. (3) Yanny et al. 1989. (4) Le Brun et al. 1997. (5) Turnshek et al. 2001. (6) Steidel et al. 1994. (7) Steidel et al. 1997.

dwarf DLA galaxy, if stars are present in the H I gas at all. Although the data set contains only 14 systems, some important trends emerge.

The b versus L/L^* plot shows that low-luminosity dwarf galaxies with small impact parameters dominate this small sample. Since DLA galaxies are H I cross section–selected, this means that sub-L^* dwarf galaxies dominate the H I cross section at $z \approx 0.5$. This is also indicated by the luminosity histogram, n versus L/L^*, which implies that it is $\approx$3 times more likely for a quasar sight line to intercept an $\approx 0.1L^*$ galaxy than an $\approx L^*$ galaxy. For galaxies at the present epoch, Zwaan, Briggs, & Verheijen (2002; see their Fig. 1) show that the probability of intercepting DLA gas, i.e., the cross-sectional area of DLA gas per unit volume, as a function of galaxy magnitude is flat for a steeply rising optical luminosity function with $\alpha = -1.5$ and decreases at faint magnitudes for $\alpha = -1.2$ or -1.0. Expressed as a function of luminosity, this probability would rise as $\sim L^{-1}$ toward the faint end for the case in which $\alpha = -1.5$ and, based on the data points in their Figure 1, would increase as $\sim L^{-0.5}$ toward the faint end for $\alpha = -1.0$. For the latter case, the trends at $z = 0$ and $z \approx 0.5$ are similar. Turnshek, Rao, & Nestor (2002) arrived at much the same conclusion (see their Fig. 4). They compared the optical diameter–limited (>7′) complete sample of $z = 0$ galaxies from Rao & Briggs (1993) to a $z \approx 0.5$ sample similar to the one in Table 4. They found that the relative absolute magnitude distributions of the two samples are comparable within the large uncertainties associated with the low-redshift sample.[3] We note that Table 4 has our final measurements for the four DLA galaxies discussed in this paper, as opposed to the preliminary measurements used in Turnshek et al. (2002). Also, the galaxy toward AO 0235+164 was not included in their analysis.

The trend that higher column densities tend to be observed at low impact parameters (b vs. $\log N_{HI}$) is not unexpected. However, what is unexpected is that the highest column densities are observed in galaxies with the lowest luminosities ($\log N_{HI}$ vs. L/L^*). This latter trend might be explained if a selection bias exists such that bright galaxies with high column densities at small impact parameters are missing from our sample. This might be caused by dimming of the background quasar due to reddening from the foreground DLA gas, excluding such bright quasars from our magnitude-limited sample. While a study by Ellison et al. (2001) on the occurrence of DLA systems at $z \approx 2$ in a radio-selected quasar sample did not show a significant excess in the DLA number density as compared to DLA systems found in optically selected quasar samples, this might not hold true at lower redshift.

[3] This statement is based on a relative comparison at the two epochs, independent of any evolution in dn/dz (which measures evolution in galaxy number density times galaxy cross section) for DLA systems (RT2000).

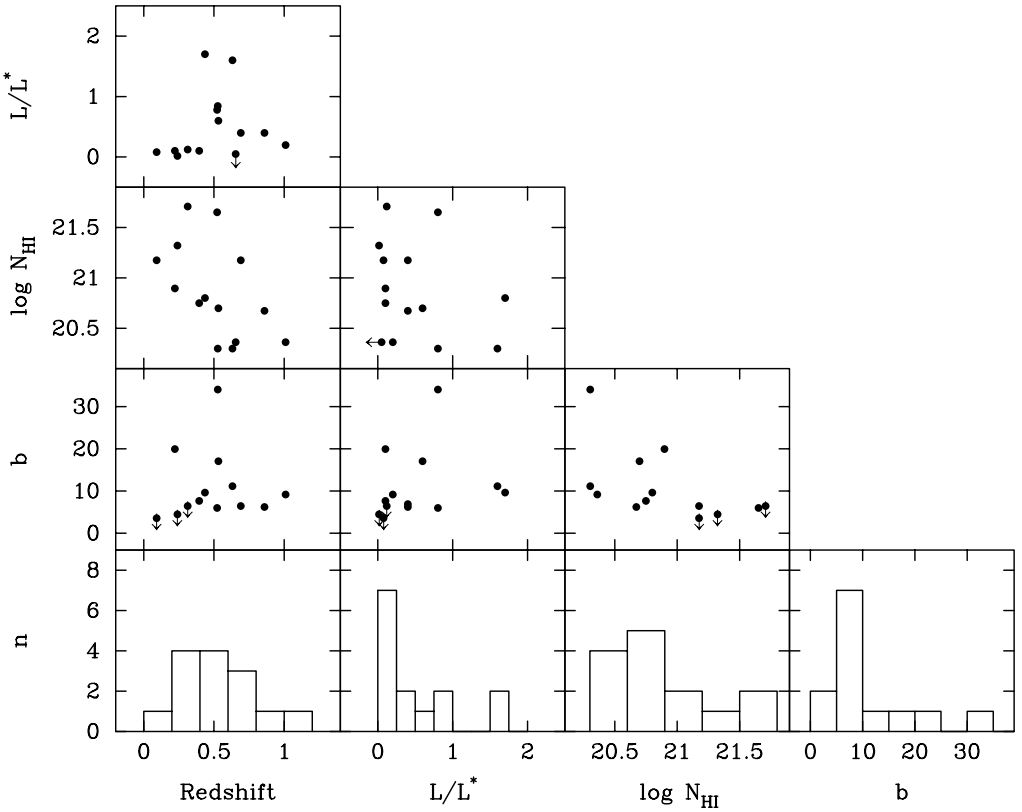

FIG. 10.—Distribution of properties for the DLA galaxies listed in Table 4. An upper limit for the luminosity of the DLA galaxy in the 3C 336 field is plotted, but an impact parameter is not, since no DLA galaxy has been detected. *B*-band luminosities are plotted in all cases except the two for which only *K*-band measurements exist. The impact parameter *b* is in kiloparsecs. Upper limits in *b* are indicated by arrows. The *b* histogram has upper limits included as measurements.

Two specific oddities of the sample are worth mentioning here: (1) Four of the five DLA galaxies with $N_{\rm H\,I} > 1 \times 10^{21}$ atoms cm^{-2} are LSB galaxies. This may have significant implications for the whereabouts of the bulk of the H I gas, since the cosmological determination of $\Omega_{\rm H\,I}$ from DLA systems is dominated by the ones with the highest column densities. These four DLA systems contain 55% of the total column density in Table 4. Zwaan et al. (2003) have shown that only 15% of the neutral gas at the present epoch is contained in LSB galaxies. Thus, if the low-redshift DLA galaxy trends hold up with larger samples, it would indicate that a different population of objects is responsible for the bulk of the neutral hydrogen gas in the universe at $z \approx 0.5$. (2) The three galaxies that have the largest impact parameters (17, 20, and 34 kpc) are spirals. G1 in the B2 0827+243 field is an $\approx L^*$ spiral galaxy and has the largest impact parameter, and, as discussed earlier, it shows signs of an interaction that might be responsible for distributing the gas to larger galactocentric distances. It was only possible to see evidence for this in the high-resolution *HST* image that exists for the field. Similar high-resolution *HST* images do not exist for the other two large–impact parameter fields, i.e., the dwarf spiral galaxy in the OI 363 field and the $\approx L^*$ spiral galaxy in the PKS 1629+120 field. Study of these two fields at higher resolution would be highly desirable in order to understand the reality and nature of this DLA gas at unusually large galactocentric distance.

We are grateful to the staff at the NOAO, and to the WIYN queue team in particular, for their assistance with the observing. We also thank the MDM observatory and IRTF support astronomers for their assistance. The ground-based component of this work has been funded in part by an NSF grant, while the space-based component of this work has been funded in part by a NASA LTSA grant. Support was also provided by NASA through a grant from the Space Telescope Science Institute, which is operated by AURA, Inc., under NASA contract NAS 5-26555. Alberto Conti is gratefully acknowledged for using his galaxy template PCA code to derive a photometric redshift for G1 in the PKS 1629+120 field. D. B. N. acknowledges partial support from a Daniels graduate student fellowship and a Mellon graduate student fellowship at the University of Pittsburgh.

APPENDIX

STELLAR POPULATION TEMPLATE FITS

In order to investigate the stellar populations present in the DLA galaxies, we fitted stellar population synthesis models to the photometry when sufficient multiband data were available. However, multiple stellar populations typically contribute to

an observed SED. Therefore, we used a fitting method that allows for contributions from multiple stellar populations attenuated by a variable amount of wavelength-dependent extinction due to dust. At the same time, galaxy colors are known to be degenerate in age-metallicity-redshift space, so further assumptions and an interpretation of what our fits mean are generally required.

First, when performing fits, we set the redshift of the galaxy to the DLA redshift. In all three cases there was reasonable justification for this. The adopted redshift was either confirmed spectroscopically or verified to be a likely photometric redshift. Second, the metallicities of all the template spectra were fixed to be solar. On the one hand, this is useful, since solar metallicity is an often-used benchmark. However, it is well known that the measured metallicities of DLA gas at moderate-to-high redshift are closer to1/10 solar. If lower metallicities (e.g., $\approx$0.2–0.02 solar) hold for the DLA galaxies studied here, the nature of the age-metallicity degeneracy means that we would generally underestimate the age of the stellar population(s) in the DLA galaxy. If the stellar metallicity were $\approx$0.2 solar, the effect would be quite small, but at metallicities as low as $\approx$0.02 solar, the effect is substantial. Thus, even with the advantage of fixing redshift, the age-metallicity degeneracy gives rise to some interpretive limitations. Another limitation is the degree to which any adopted set of template spectra (see below) are applicable to fit the observed SEDs. In any case, when the qualitative results of the SED fitting are taken in combination with morphological information, we are generally able to draw a consistent conclusion that provides useful information on the evolutionary history of a DLA galaxy as presented in § 3.

For the template spectra we use the galaxy isochrone synthesis spectral evolution library (GISSEL99) of G. Bruzual A & S. Charlot (2003, in preparation). We chose templates with a Scalo initial mass function (IMF) corresponding to instantaneous bursts observed at 11 different ages: 10^{-3}, 10^{-2}, 0.05, 0.1, 0.2, 0.3, 0.6, 1.0, 1.5, 4, and 12 Gyr. From these original 11, we generated an additional 110 templates by applying a Calzetti reddening law (Calzetti et al. 2000) with 10 different dust extinction values, corresponding to $E(B-V)$ of 0.05, 0.1, 0.2, 0.3, 0.4, 0.5, 0.6, 0.7, 0.8, and 0.9. The convolution of each of these 121 redshifted templates with the *UBRJK* filter set (*UBRIK* for B2 0827+243) was converted to flux units, resulting in a flux 5-vector for each template. Models were then built to minimize the χ^2 fit to the observed photometric SEDs for each of the $121!/(121-N)!N!$ combinations of N 5-vectors, where N was the number of component templates used in the fit. We investigated cases in which the value of N was 1, 2, or 3. The model that gave the most reasonable value for reduced χ^2 was then reported as the most likely (combination of) stellar population(s) in a galaxy. For example, both single- and two-burst models are reported as best fits to the photometry of G1 in the B2 0827+243 field, while a single-burst model was clearly appropriate for fitting the photometry of G1 in the PKS 1629+120 field (i.e., a two-burst model had a noticeably larger reduced χ^2). Although we explored three-burst models, the resulting improvements in reduced χ^2 values did not justify their use.

The standard interpretation of reduced χ^2 fitting results holds for the best fits presented in § 3. That is, if the adopted template spectra are representative of our observed SEDs and if our derived observational errors are valid, model fits that have a reduced χ^2 between $\approx$0.8 and 2 (which correspond to reduced χ^2 probabilities between $\approx$0.5 and 0.2) are taken to be acceptable fits. On the other hand, a reduced χ^2 value much larger than this should formally be rejected. There are two possible reasons for this. Either (1) the errors have been underestimated, which might be the case if some unknown systematic error in some of the photometry exists, or (2) the set of template spectra used to fit the observed SEDs is inappropriate. We suspect that in cases in which we have a larger reduced χ^2, say $\approx$5, the quoted fits still provide qualitative information on the nature of the DLA galaxy's stellar population. It might be that the χ^2 could be reduced further by assuming some specific form for time-variable star formation, and/or by using different metallicities, and/or by tracking down an unknown systematic error in the photometry. Another possibility is finding a reduced χ^2 value much less than 1 (resulting in a probability greater than 0.5). This may be indicative of overfitting the data or error estimates that are too large.

The specifics of the various fits to DLA galaxy SEDs are discussed in § 3. Models that included a negative population were rejected as unphysical. Quoted fractions are by burst mass, although one should keep in mind that any such method is sensitive only to the light output of the galaxy, and as younger populations will have smaller mass-to-light ratios, large old populations may not be resolved by this technique when a large young burst is present. As noted above, instantaneous bursts may be unreliable approximations for star formation histories of real galaxies in many cases. By building the best-fit model from multiple templates, however, we in effect mimic a nonparametric star formation history. Nonetheless, we repeated the process with sets of exponentially decreasing star formation rates. The results from the two methods were consistent. For example, a galaxy that showed an equal combination of old and young stellar populations from our first method would show a long e-folding time in the second method, while a galaxy with a predominately young population would show a very short e-folding time.

REFERENCES

Afonso, J., Mobasher, B., Chan, B., & Cram, L. 2001, ApJ, 559, L101
Aldcroft, T. L., Bechtold, J., & Elvis, M. 1994, ApJS, 93, 1
Barthel, P. D., Tytler, D. R., & Thomson, B. 1990, A&AS, 82, 339
Bergeron, J., & Boissé, P. 1991, A&A, 243, 344
Binggeli, B., Popescu, C. C., & Tammann, G. A. 1993, A&AS, 98, 275
Bouché, N., Lowenthal, J. D., Charlton, J. C., Bershady, M. A., Churchill, C. W., & Steidel, C. C. 2001, ApJ, 550, 585
Bowen, D. V., Tripp, T. M., & Jenkins, E. B. 2001, AJ, 121, 1456
Burbidge, E. M., Beaver, E. A., Cohen, R. D., Junkkarinen, V. T., & Lyons, R. W. 1996, AJ, 112, 2533
Calzetti, D., Armus, L., Bohlin, R. C., Kinney, A. L., Koornneef, J., & Storchi-Bergmann, T. 2000, ApJ, 533, 682
Cimatti, A., Villani, D., Pozzetti, L., & di Serego Alighieri, S. 2000, MNRAS, 318, 453
Cimatti, A., et al. 1999, A&A, 352, L45
Cowie, L. L., Gardner, J. P., Hu, E. M., Songaila, A., Hodapp, K.-W., & Wainscoat, R. J. 1994, ApJ, 434, 114
Daddi, E., Cimatti, A., & Renzini, A. 2000, A&A, 362, L45
Dey, A., Graham, J. R., Ivison, R. J., Smail, I., Wright, G. S., & Liu, M. C. 1999, ApJ, 519, 610
Ellison, S. L., Yan, L., Hook, I. M., Pettini, M., Wall, J. V., & Shaver, P. 2001, A&A, 379, 393
Haehnelt, M. G., Steinmetz, M., & Rauch, M. 1998, ApJ, 495, 647
Hamilton, T. S., Casertano, S., & Turnshek, D. A. 2002, ApJ, 576, 61
Jannuzi, B. T., et al. 1998, ApJS, 118, 1

Kanekar, N., & Chengalur, J. N. 2001a, A&A, 369, 42
———. 2001b, MNRAS, 325, 631
Kukula, M. J., Dunlop, J. S., McLure, R. J., Miller, L., Percival, W. J., Baum, S. A., & O'Dea, C. P. 2001, MNRAS, 326, 1533
Lane, W. 2000, Ph.D. thesis, Univ. Groningen
Lane, W., Smette, A., Briggs, F., Rao, S., Turnshek, D., & Meylan, G. 1998, AJ, 116, 26
Lanzetta, K. M., Wolfe, A. M., Turnshek, D. A., Lu, L., McMahon, R. G., & Hazard, C. 1991, ApJS, 77, 1
Le Brun, V., Bergeron, J., Boissé, P., & Deharveng, J. M. 1997, A&A, 321, 733
Lin, H., Kirshner, R. P., Shectman, S. A., Landy, S. D., Oemler, A., Tucker, D. L., & Schechter, P. L. 1996, ApJ, 464, 60
Loveday, J. 2000, MNRAS, 312, 557
Madau, P., Pozzetti, L., & Dickinson, M. 1998, ApJ, 498, 106
Marinoni, C., Monaco, P., Giuricin, G., & Costantini, B. 1999, ApJ, 521, 50
McDonald, P., & Miralda-Escudé, J. 1999, ApJ, 519, 486
Péroux, C., McMahon, R. G., Storrie-Lombardi, L. J., & Irwin, M. J. 2001, MNRAS, submitted (astro-ph/0107045)
Poggianti, B. M. 1997, A&AS, 122, 399
Pozzetti, L., & Mannucci, F. 2000, MNRAS, 317, L17
Prochaska, J. X., & Wolfe, A. M. 1997, ApJ, 487, 73
———. 1998, ApJ, 507, 113
Rao, S. M., & Briggs, F. H. 1993, ApJ, 419, 515
Rao, S. M., & Turnshek, D. A. 1998, ApJ, 500, L115
———. 2000, ApJS, 130, 1 (RT2000)
Rao, S. M., Turnshek, D. A., & Briggs, F. H. 1995, ApJ, 449, 488
Smith, G. P., Treu, T., Ellis, R., Smail, I., Kneib, J.-P., & Frye, B. L. 2001, ApJ, 562, 635
Steidel, C. C. 1993, in The Environment and Evolution of Galaxies, ed. J. M. Shull & H. A. Thronson, Jr. (Dordrecht: Kluwer), 263
Steidel, C. C., Dickinson, M., Meyer, D. M., Adelberger, K. L., & Sembach, K. R. 1997, ApJ, 480, 568
Steidel, C. C., Kollmeier, J. A., Shapley, A. E., Churchill, C. W., Dickinson, M., & Pettini, M. 2002, ApJ, 570, 526
Steidel, C. C., Pettini, M., Dickinson, M., & Persson, S. E. 1994, AJ, 108, 2046
Turnshek, D. A., Rao, S., & Nestor, D. 2002, in ASP Conf. Ser. 254, Extragalactic Gas at Low Redshift, ed. J. Mulchaey & J. Stocke (San Francisco: ASP), 42
Turnshek, D. A., Rao, S., Nestor, D., Lane, W., Monier, E., Bergeron, J., & Smette, A. 2001, ApJ, 553, 288
Turnshek, D. A., Rao, S. M., Ptak, A. F., Griffiths, R. E., & Monier, E. M. 2003, ApJ, 590, 730
Warren, S. J., Møller, P., Fall, S. M., & Jakobsen, P. 2001, MNRAS, 326, 759
Wolfe, A. M., Turnshek, D. A., Smith, H. E., & Cohen, R. D. 1986, ApJS, 61, 249
Yanny, B., York, D. G., & Gallagher, J. S. 1989, ApJ, 338, 735
Zwaan, M., Briggs, F. H., & Verheijen, M. 2002, in ASP Conf. Ser. 254, Extragalactic Gas at Low Redshift, ed. J. Mulchaey & J. Stocke (San Francisco: ASP), 169
Zwaan, M., et al. 2003, AJ, 125, 2842